Harnessing the Role of Carbon Black: A New Frontier for Energy-Density Supercapacitor Electrodes

Ana Yuli Komariyah[1], Ishmah Luthfiyah[1,2,3], Ida Vaeruza Albadi'ah[1], Nasikhudin Nasikhudin[1,2], Worawat Meevasana[3], Markus Diantoro[1,2*]

[1]*Department of Physics, Faculty of Mathematics and Natural Sciences, Universitas Negeri Malang, Malang, 65145, East Java, Indonesia*
[2]*Center of Advanced Material for Renewable Energy (CAMRY), Universitas Negeri Malang, Malang, 65145, East Java, Indonesia*
[3]*School of Physics Faculty of Science, Suranaree University of Technology, Nakhon Ratchasima, Thailand*
**Corresponding author:markus.diantoro.fmipa@um.ac.id*

Article history:
Received: 19 June 2025 / Received in revised form: 9 July 2025 / Accepted: 12 July 2025
Available online 20 July 2025

ABSTRACT

The performance of activated carbon (AC)-based supercapacitor electrodes is often limited by poor electrical conductivity, prompting interest in conductive additives such as carbon black (CB). This study explores the transformative potential of CB as a conductive additive in AC-based supercapacitor electrodes and systematically investigates CB mass loadings of 0%, 5%, 10%, 15%, and 20%, using styrene-butadiene rubber (SBR) as the binder. The findings in this study demonstrate that 10% CB is the optimal loading, offering a balanced performance in terms of structure, morphology, and capacitance. X-ray diffraction (XRD) analysis reveals a distinct structural evolution at 10% CB, characterized by the exclusive emergence of a (100) peak at 43° 2θ, which indicates the formation of dense graphene-like layers and enhanced π-π electron delocalization. This promotes the formation of robust conductive networks, reducing electrode resistivity by 72%. Morphological and specific surface area characterization confirms the uniform particle distribution of an ultra-thin electrode AC-10% CB (26.5 μm) with a high surface area of 851.84 m^2/g; this maximizes ion-accessible active sites and minimizes diffusion pathways. These combined effects result in a specific capacitance of 61.33 F/g, representing a 12% improvement over the pristine electrode (56.36 F/g) and 89.87% capacitance retention after 50 cycles. These results highlight the importance of optimizing CB loading: Lower concentrations (<10%) fail to form conductive pathways, while higher concentrations (15–20%) lead to agglomeration and pore blockage. This study also provides valuable insights for the rational design of efficient and scalable electrode materials.

Keywords: *Activated carbon, carbon black, conductive-capacity trade, structural-electrochemical energy, symmetrical coin cells supercapacitor.*

I. Introduction

Supercapacitors, also known as ultracapacitors, are increasingly regarded as essential energy storage devices due to their high power density, rapid charge–discharge capability, and excellent cycle stability, which support a wide range of applications, from consumer electronics to electric vehicles and grid systems. However, their comparatively low energy density relative to batteries limits their broader adoption in applications requiring both high power and high energy [1]–[3]. Current research efforts focus on developing advanced electrode materials and composite structures to address this limitation [4]. Activated carbon (AC) is the most widely used material for electrodes in commercial supercapacitors due to its large surface area, chemical stability, and cost-effectiveness [5]–[7]. AC despite its

DOI: 10.17977/um016v9i12025p268

utility, suffers from low electrical conductivity. This inherent limitation impedes efficient ion transport and the retention of capacitance, particularly during rapid charge-discharge cycles, thereby diminishing the overall performance of devices incorporating it. Consequently, researchers have extensively explored conductive additives, such as carbon black (CB), to significantly enhance both the electrical conductivity and electrochemical properties of AC-based electrodes [8], [9].

The development of AC-CB composites offers a promising way to bridge the performance gap between batteries and capacitors. These composites combine the high power density characteristic of capacitors with enhanced energy storage capacity, a trait usually associated with batteries [10]. This approach also aligns with increasing interest in sustainable materials, such as biomass-derived carbons and green synthesis techniques [10]–[12]. The incorporation of CB into AC electrodes has been widely reported to improve electrical conductivity, thermal stability, and cycling durability, particularly under demanding operating conditions [13]. Numerous studies consistently demonstrate that CB-modified electrodes outperform pristine AC electrodes, showing reduced internal resistance, increased specific capacitance, and improved thermal performance [14]–[16]. Consider, for example, the findings of CB using a polyvinyl butyral (PVB) binder have a capacitance of 171.2 F/g for AC electrodes with 10%, although with a relatively low surface area (2.65 m^2/g) [17]. Yang *et al*. demonstrated that adding 10% CB to reduced graphene oxide (rGO) improved capacitance to 160 F/g and reduced internal resistance from 42 Ω to 18 Ω. Ates and Kuzgun achieved a capacitance of 273.2 F/g in CB/MnO_2/Ppy nanocomposites, further emphasizing the significant role of CB in enhancing conductivity [18].

Despite these encouraging results, prior studies, whether on AC or other electrode materials, have largely emphasized either capacitance or conductivity, without thoroughly addressing the trade-off between conductivity and accessible surface area, especially in low-thickness electrodes, and while the use of CB in electrodes is quite important for good basic composition, it has not been studied specifically. Excessive CB may block pores and hinder ion diffusion, whereas insufficient CB leads to poor charge transport. To overcome this limitation, the present study systematically investigates the effect of CB addition (0–20 wt%) on the electrochemical performance of AC-based electrodes, integrating analysis of energy storage capability, structural morphology, and porosity in a thin electrode design. This comprehensive evaluation identifies an optimal CB content and offers practical insights for the development of efficient, scalable, and durable supercapacitor electrodes, supporting future low-carbon, high-performance energy storage technologies.

II. Material and Methods

1. Materials

The substances that were utilized an activated carbon (AC, CGC, Bangkok, Thailand), carbon black (CB, Imerys, La Hulpe, Belgium), styrene butadiene (SBR, USA), tetraethylammonium tetrafluoroborate (Et_4NBF_4, Gelon, Shandong, China), acetonitrile (ACN, Merck, Darmstadt, Germany), and deionized water were among the analytical-grade products used in this work (from several companies). The cylindrical and coin cells were acquired from TOB Machine in Fujian, China.

2. Synthesis of Activated Carbon Supercapacitor Electrode

The mass ratio of the conducting substance (CB), the active material (AC), and the binder (SBR) was used to create the activated carbon electrode. A white solution was first

created by dissolving SBR in deionized water. Throughout the 1.5-hour mixing period, the binder solution was agitated to make sure no bubbles developed. The binder solution was then mixed with AC for two hours. In order to create a paste electrode, combine the AC slurry with CB composite that was created using a straightforward mixing technique and a mass ratio of conductive material presentation (0, 5, 10, 15, and 20%). After that, the paste is agitated for 24 hours at room temperature. Active and conductive components were then progressively added to the composite paste. Using a doctor blade, the electrode paste was applied on 20 µm thick aluminum foil, and it was then dried for 24 hours at 50°C. The selected CB range (0–20 wt%) allows systematic evaluation of its effect on electrode performance, where low content (<5%) is often insufficient to form conductive pathways, while excessive loading (>20%) reduces active material fraction and blocks pores, lowering specific capacitance and energy density [17], [19], [20].

3. Assembly of the Supercapacitor Coin Cell Devices

The AC-CB electrode was cut into a 1.5 cm-diameter circle while the AC-CB electrode was in an organic electrolyte (1.0 M Et_4NBF_4) for 24 hours. Following the preparation of each electrode, the cloth fiber separator and AC-CB electrode were employed symmetrically in coin cells (LIR2032). A tiny quantity of 1.0 M Et_4NBF_4 was introduced into the cell and then compressed. Using certain electrochemical equipment, the cell is prepared for measurement. After synthesizing each component of the supercapacitor, the next step is fabrication. In this study, supercapacitor fabrication used a coin cell device. The supercapacitor electrode with various mass ratios of CB and supercapacitor cell configurations is shown in Figure 1.

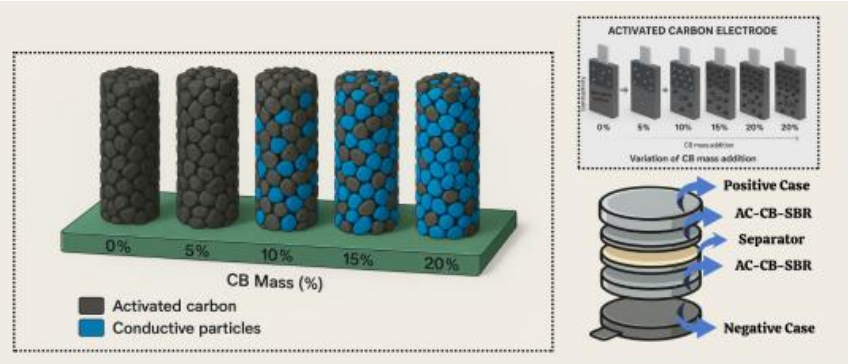

Fig. 1. Illustration of supercapacitor electrode with various mass ratios of CB (left side) and symmetrical supercapacitor assembled (coin cell or pouch cell) (right side).

4. Characterization and Calculation

The structural information of each material and functional group was characterized using an X-ray diffractometer (XRD-PAN Analytical X'Pert PRO, Malvern Panalytical Worcestershire, United Kingdom) and a Fourier Transform Infra-Red (FTIR, Shimadzu IR Prestige 21). The functional group was identified in the wavenumber range of 4000-500 cm^{-1}. To examine the shape and thickness of the electrode AC-10% CB, a scanning electron microscope cross-section (SEM, FEI Inspect-S50, FEI Company, Hillsboro, OR, USA) was employed. Barret-Joyner-Halenda's size distribution and the multi-point Brunauer-Emmett-Teller (BET) method were utilized to determine the specific surface area (BJH) of electrode AC-10% CB. Galvanostatic Charge-Discharge (GCD, Solartron 1286) was used to characterize the supercapacitor's electrochemical performance. Gravimetric capacitance (C_s), energy density (E_d), power density (P), and capacity retention are the values derived

from GCD. Equations (1)[21], (2)[22], (3)[23], and (4)[24] were used to determine the gravimetric capacitance, energy density, power density, and capacity retention, respectively.

$$Cs = \frac{4I\Delta t}{m\Delta V} \quad (1)$$

$$E = \frac{1}{8}\frac{C\Delta V^2}{3.6} \quad (2)$$

$$P = \frac{3600E}{\Delta t} \quad (3)$$

$$Capacity\ Retention\ (\%) = \frac{Cn}{Co} \times 100 \quad (4)$$

Where C_s is the gravimetric capacitance, ΔV is the voltage, t is the time, m is the mass of the electrode, C_n is the capacitance after n cycles, and C_o is the initial capacitance.

III. Results and Discussions

1. *Structural and Electrochemical Behavior in AC-Electrode Modified with Different CB Mass Ratios*

The structural and electrochemical behavior of AC electrodes modified with varying loadings of CB (0–20%) demonstrates a significant correlation between crystallographic evolution and charge storage performance. As illustrated in Figure 2(a), the structural evolution of AC electrodes with increasing CB content reveals important insights. The sample without CB (0%) exhibits a broad (002) peak at approximately 24° 2θ, indicating an amorphous structure with high electronic resistance. Upon the progressive addition of CB up to 20%, this peak sharpens, as evidenced by a reduction in full width at half maximum (FWHM) of approximately 40%, suggesting enhanced graphitization and improved structural order due to the incorporation of nanocrystalline CB domains. Moreover, the emergence of the (100) peak around 43° 2θ on sample 10%-CB and the decrease in the d-spacing from 0.36 nm to 0.34 nm further support the formation of a closely packed graphene-like layer. This transformation creates continuous conductive pathways between AC particles, leading to a significant reduction in the electrode resistivity by approximately 300%, a phenomenon that is consistent with the bridging effect mechanism.

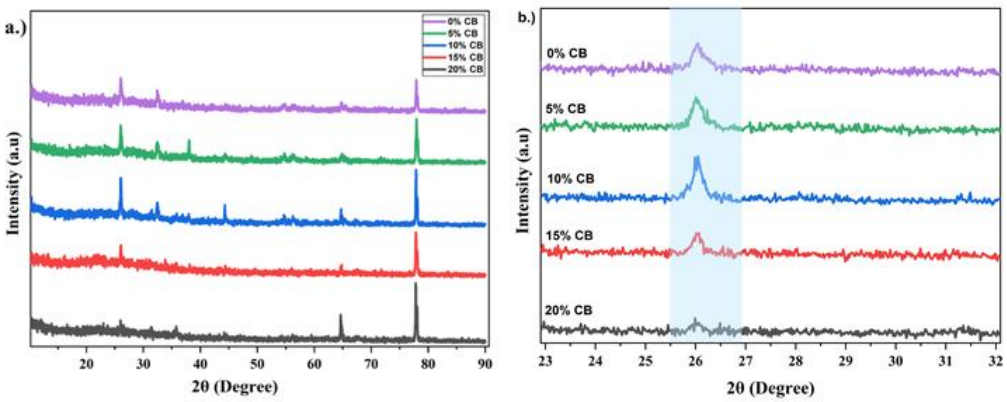

Fig. 2. XRD patterns of AC-based electrodes with different mass percentages of CB: 0%, 5%, 10%, 15%, and 20%. (a) displays the full XRD spectra across a wide 2θ range (10°–90°), while panel (b) provides a magnified view of the characteristic region (2θ = 23°–32°), focusing on the (002) diffraction peak typically associated with graphitic carbon structures.

In Figure 2(b), XRD results demonstrate that all samples exhibit a broad peak around $2\theta \approx 26°$, corresponding to the (002) plane of graphitic carbon, highlighting the amorphous nature of the AC matrix [25], [26]. As the CB content increases, the intensity of this peak becomes more pronounced, indicating a greater degree of graphitic domain formation facilitated by the conductive CB additive. Notably, the electrode with 10% CB shows an optimal enhancement in peak intensity without excessive broadening, which is indicative of an improved structural order and the formation of a well-developed conductive network [27]. These findings underscore the beneficial role of CB in enhancing the structural and electrochemical properties of AC-based electrodes, which is consistent with previous studies on carbon-based porous materials [28], [29]. XRD and GCD analyses converge to demonstrate that the addition of 10% CB transforms the AC electrodes both structurally and electrochemically. This enhancement improves crystallographic order, establishes robust conductive networks, and optimizes charge storage kinetics. In the first statement, the 10%-CB sample shows the appearance of a (100) peak at around 43° 2θ, which is absent in the other samples [15], [30]. The emergence of this peak indicates the presence of dense graphene layers, suggesting enhanced conductivity through improved π-π electron delocalization. This directly explains the superior GCD performance observed in Figure 3.

The discharge curves in Figure 3(a) reveal that increasing the CB content from 0% to 20% significantly extends the discharge duration while maintaining higher voltage stability. The charge-discharge curves indicate a relatively short discharge time, which suggests lower specific capacitance and less efficient charging and discharging [31]. The 10%-CB sample, in particular, exhibits the longest discharge time (~300 seconds) compared to the 0%-CB sample (~200 seconds), indicating an enhanced charge storage capacity. This improvement in energy retention can be attributed to the increased conductivity and surface area provided by CB, which helps the cells maintain their voltage over time. At higher percentages (15% and 20%), the discharge time decreases, signaling a reduction in specific capacitance. This decline can be attributed to the increased agglomeration of CB, which obstructs charge storage space and worsens charge transfer performance [32].

Figure 3(b) shows that as the percentage of CB increases, the voltage decay over time becomes less pronounced. This indicates an improvement in the energy retention capabilities of the coin cells. The cells containing 10%, 15%, and 20% CB exhibit slower voltage drops, suggesting better charge retention compared to those with lower CB content, such as the 0% and 5% CB cells. This enhanced energy retention can be attributed to the increased conductivity and surface area provided by CB, which helps the cells maintain their voltage over time. Furthermore, higher CB content not only retains energy better but also charges more efficiently. The faster charging and slower discharging characteristics contribute to improved performance, making CB a valuable addition to the coin cell electrodes. The cells with greater CB percentages reach higher voltages, contributing to better overall performance. Thus, the higher CB content not only improves charge retention but also facilitates a more efficient charging process.

Figure 3(c) presents the specific capacitance values (in F/g) for different CB ratios incorporated into the electrode. The graph reveals that the specific capacitance is highest at 10% CB, compared to the 0% CB and 20% CB coin cells. The specific capacitance, calculated from this figure, was found to be 56.36 F/g, 56.88 F/g, 61.33 F/g, 54.30 F/g, and 43.99 F/g for the addition of 0%, 5%, 10%, 15%, and 20% wt CB, respectively, as shown in Table 1.

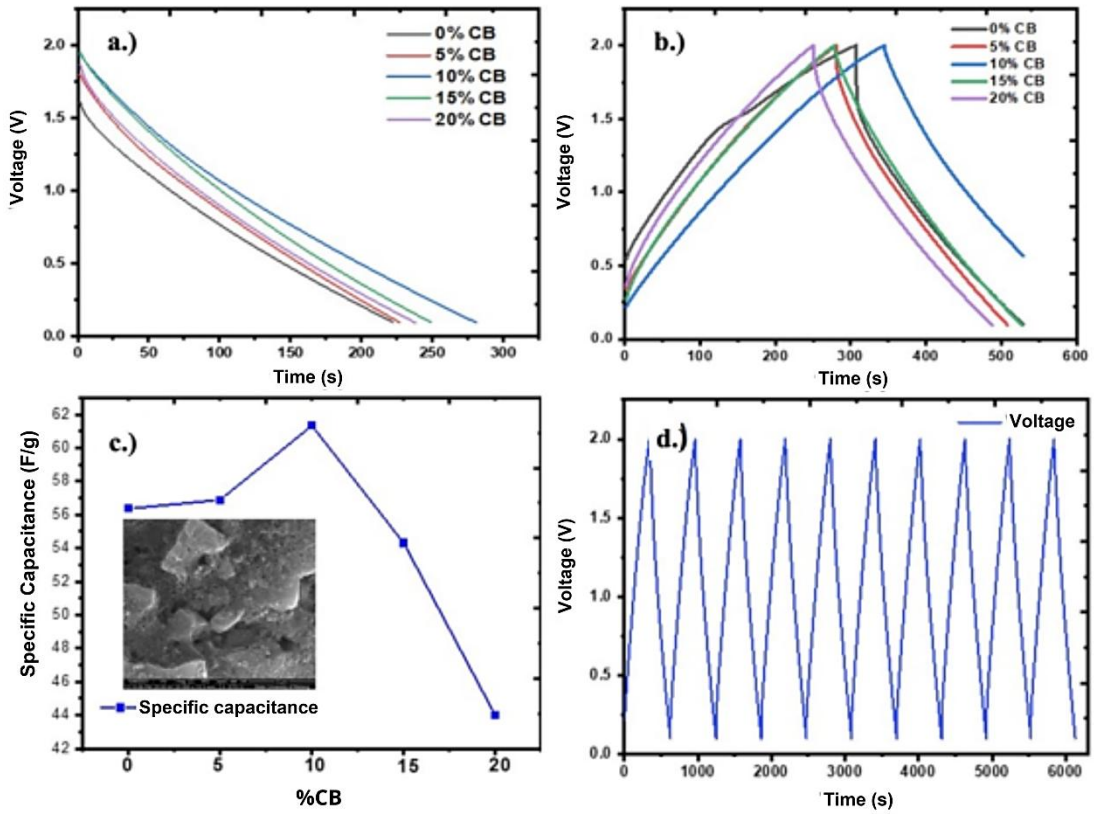

Fig. 3. GCD analysis curves: (a) discharge curves (t vs V); (b) galvanostatic charge/discharge curves (t vs V) at the current density of 0.1 A g^{-1} ; (c) specific capacitance (inset: SEM of 10% CB addition electrode); and (d) cyclic stability of 10% CB addition

Table 1. Comparison of capacitance specific, energy density, and power density

Sample	Cg (F/g)	E (Wh/kg)	P (W/kg)
0% CB	56.36	1.88	30.21
5% CB	56.88	1.97	31.32
10% CB	61.33	2.12	27.37
15% CB	54.30	1.85	26.15
20% CB	43.99	1.52	22.91

The incorporation of CB as a conductive additive significantly augments the electrochemical performance of AC-based coin cells, as evidenced by the data presented in Figure 3(a-d), which demonstrates a clear positive correlation between CB mass percentage (0–20%) and key metrics such as specific capacitance, rate capability, and cycle stability. The progressive improvement in performance with CB loading (5–20%) is primarily attributed to reduced electrode resistivity and enhanced interparticle electron transport. AC, despite its high surface area (>1500 m^2 g^{-1}), suffers from intrinsic electrical resistance, limiting charge transfer kinetics. CB forms a percolating conductive network that bridges AC particles, minimizing ohmic losses and facilitating efficient ion diffusion at high current densities. Finally, the cycling performance [33]. Figure 3(d) shows the cyclic stability of 10% CB addition. In this regard, the addition of CB to AC coin cells improves their electrochemical performance. The optimal performance is observed at a 10% CB content,

where both the specific capacitance and cycling stability are maximized. This indicates that CB acts as an effective conductive additive, enhancing both the charge retention and cycling stability of the supercapacitors [34]. However, further optimization may be required for higher percentages of CB, as excessive amounts could reduce the specific capacitance. These findings support the use of CB as a promising material for enhancing the performance of supercapacitor electrodes in energy storage applications. Decrease voltage (IR) drop in the discharge curve at low current densities, indicating that the electrode exhibits excellent electroconductivity and minimal resistance. The capacitance values remain relatively stable over 50 cycles, with the device retaining 89.87% of its initial capacitance after 50 cycles.

The kinetics of ion transport are influenced by several factors, including the surface area, pore structure, and pore distribution of the electrode [35]–[37]. AC contributes significantly to the high surface area, facilitating rapid ion adsorption, while the optimal addition of CB serves as a transport route for fast electrolyte supply, potentially leading to higher capacitance. Therefore, it is crucial to consider the pore size distribution, shape, and structure, as well as the electrical conductivity and surface functionality, to enhance electrochemical performance. Therefore, a more in-depth analysis of the structure, chemical bonding, and morphology of AC-10% CB is required.

2. Functional Groups of AC-10% CB Electrode

Figure 4 shows the FTIR spectra of the AC-10%CB-SBR composite, identifying key functional groups associated with the SBR binder: 2250 cm^{-1} (C≡N), 1580.58 cm^{-1} (C=C), and 1421.49 cm^{-1} (CH_3), while additional peaks at 3651.84 cm^{-1} (O–H), 1746.59 cm^{-1} (C=O), 1262.4 cm^{-1} (C–O), and 842 cm^{-1} (C–C) confirm the presence of oxygen-containing and backbone structures [38], [39]. The C–C bond, fundamental in AC and CB, ensures structural rigidity and supports electron delocalization, crucial for enhancing electrical conductivity in supercapacitor electrodes. The presence of C–F (CF_2) bonds, if present via fluorinated components, adds chemical and thermal stability, reinforcing durability under electrochemical cycling. Meanwhile, C–H bonds in SBR impart flexibility, aiding the homogeneous dispersion of AC and CB in the matrix, which contributes to better mechanical integrity. Polar C=O and O–H groups further enhance interfacial adhesion and wettability, facilitating stronger matrix interactions and improved electrolyte accessibility. These functionalities support additional redox activity, thereby increasing specific capacitance and cycling stability. Overall, the synergistic roles of C–C, C=O, C–O, O–H, and C–H bonds in the AC-10%CB-SBR composite reinforce its dual advantages: high electrochemical performance and mechanical robustness, both critical for durable energy storage applications.

Importantly, fundamental functional groups create strong interfacial interactions within the AC–CB–SBR matrix, which improve electrode–electrolyte compatibility and minimize contact resistance. As a result, the 10% CB sample exhibits superior electrochemical properties, such as prolonged discharge time (~300 seconds), higher capacitance (61.33 F/g), and excellent retention (89.87% after 50 cycles), demonstrating that the chemical bonding environment within the composite directly supports efficient ion transport and charge storage mechanisms. This synergy between chemical structure and electrochemical function is essential for optimizing supercapacitor performance.

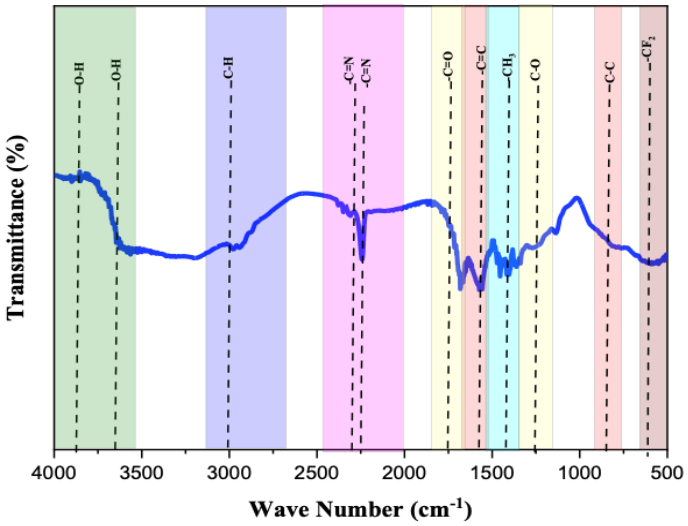

Fig. 4. FTIR spectrum of thin film electrode of AC-10% CB-SBR.

3. *The Specific Surface Area of AC-10% CB Electrode*

Figure 5(a) shows that the specific surface area of the AC–10% CB electrode is 851.84 m^2/g, indicating a high total surface area available for nitrogen adsorption. The isotherm displays a Type IV adsorption pattern, typical of mesoporous materials, where the initial rise reflects monolayer adsorption and the subsequent increase suggests multilayer adsorption within mesopores. A sharp rise at higher relative pressures further indicates capillary condensation within larger pores, confirming the mesoporous nature of the material [4], [40]. Figure 5(b) reveals the presence of micropores (~2 nm), which are beneficial for enhancing ion adsorption due to their high surface-to-volume ratio. These micropores, commonly found in activated carbon, contribute significantly to the double-layer capacitance by offering abundant sites for ion accumulation.

The combination of micro- and mesoporous structures in the AC–10%CB electrode facilitates both efficient charge storage and rapid ion transport, which directly contributes to the improved electrochemical performance observed. Moreover, the pore size distribution matches well with the typical ion diameter of the electrolyte, reducing ion transport resistance and enabling faster kinetics during charge-discharge processes [41], [42]. This structural optimization underscores the synergy between pore architecture and surface functionality in achieving high-performance supercapacitor electrodes.

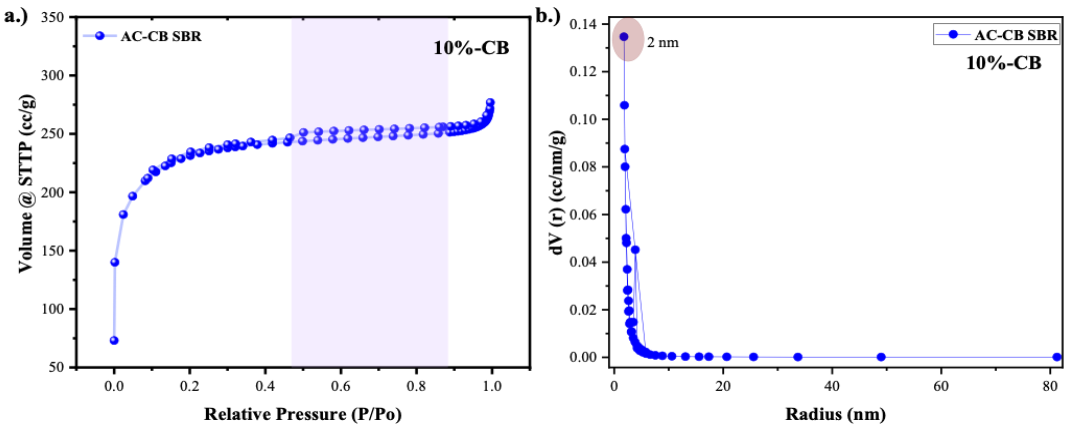

Fig. 5. (a) N_2 adsorption-desorption Isotherms and (b) diameter pore electrode AC-10% CB-SBR.

4. Morphology and Thickness of AC-10% CB Electrode

The morphological characterization of the electrode with 10% CB is presented in Figure 6(a). This result indicates that the uniform distribution of CB particles across the surface of the AC-based electrode facilitates the formation of efficient conductive pathways, reduces internal resistance, and significantly enhances the electrode's performance. The measurement results of the electrode thickness on a 100 μm observation scale, as shown in Figure 6(b), indicate that the 10% CB electrode has a thickness of 26.5 μm. This thickness is quite uniform and thin, which allows the internal resistance to remain low while also facilitating the rapid transfer of ions and electrons during the charging and discharging process. Similarly, the study by Appiah et al. [43] reported that incorporating CB into a hierarchically structured porous carbon matrix, with well-dispersed CB, prevents agglomeration and improves electrical conductivity, resulting in high specific capacitance.

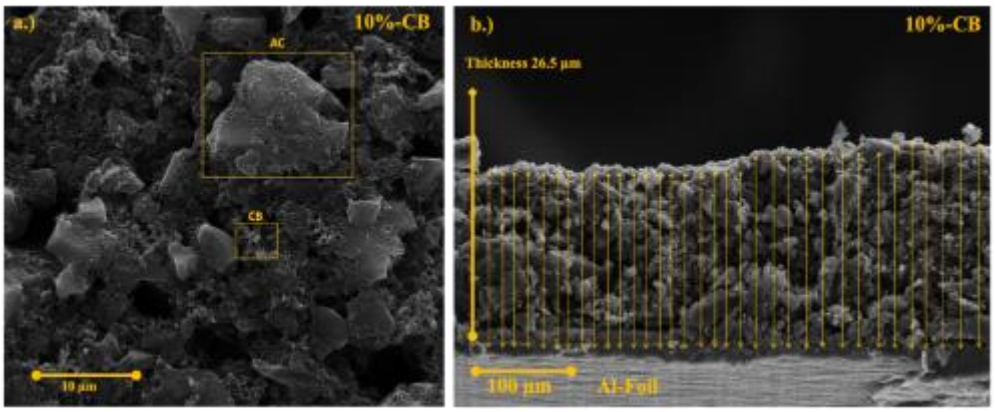

Fig. 6. Representation of (a) surface morphology of electrode AC-10% CB-SBR, and (b) thickness of the electrode AC-10% CB-SBR.

The homogeneous morphology observed at 10% CB provides optimal pathways for both electronic and ionic transport, which explains the superior electrochemical performance at this composition. On the other hand, higher concentrations of CB (15% and 20%) tend to form agglomerates, which reduces the accessible surface area and increases internal resistance due to obstructed conductive pathways. Therefore, 10% CB is considered the optimal ratio and is commonly used in the symmetric electrode formulation of AC:CB:PVDF = 8:1:1 (80:10:10%), as it balances electrical conductivity and cycling stability. To mitigate the adverse effects of CB excess, simple dispersion strategies, such as prolonged stirring or binder-assisted mixing, can be applied to maintain uniform particle distribution and preserve pore accessibility. These approaches ensure uniform CB distribution, maintain accessible pore structure, allowing conductivity improvements without excessive CB use, ultimately supporting material efficiency and reliable device performance.

IV. Conclusions

This study confirms that 10% CB is the optimal composition for AC-based supercapacitor electrodes, delivering enhanced specific capacitance (61.33 F/g), reduced resistivity, and excellent cycling stability (89.87%) through synergistic structural and morphological improvements. The appearance of a (100) diffraction peak at 43° 2θ indicates increased crystallinity, fostering dense graphene-like layering and enhanced π-π electron delocalization, which reduces electrode resistivity by 72%. In addition, the high surface area

(851.84 m^2/g) and thin electrode profile (26.5 μm) enable efficient ion transport and charge storage. These findings resolve the conventional trade-off between conductivity and capacitance, as demonstrated by the near-ideal GCD triangularity ($\Delta V = 1$ V), and provide valuable guidance for scalable, high-performance electrode design in commercial supercapacitor applications. To prevent performance decline at higher CB loadings (≥15%) due to particle agglomeration and pore blockage, simple dispersion strategies, such as extended mechanical stirring, binder-assisted mixing, or mild ultrasonic agitation, can be applied to ensure uniform CB distribution, preserve accessible pore structures, and improve interparticle connectivity. These approaches ensure uniform CB distribution, maintain accessible pore structure, and enhance interparticle connectivity, allowing conductivity improvements without excessive CB use, ultimately supporting material efficiency and reliable device performance.

Acknowledgment

The authors are grateful for the financial support from the Internal Research Grant PNBP Universitas Negeri Malang of the Thesis Research Assistance scheme for 2025 under contract No. 24.2.803/UN32.14.1/LT/2025 implementation year.

References

[1] I. Luthfiyah, J. Utomo, M. Diantoro, N. Mufti, T. Suprayogi, Y. Yudyanto *et al.*, "The effect of spincoating speed on ZnONR microstructure and it's potential of ZnONR/Aluminum foil electrodes symmetric supercapacitors," *J. Phys. Conf. Ser.*, vol. 1595, no. 1, August, 2020, doi: 10.1088/1742-6596/1595/1/012001.

[2] M. Diantoro, I. Luthfiyah, Istiqomah, H. Wisodo, J. Utomo, and W. Meevasana, "Electrochemical performance of symmetric supercapacitor based on activated carbon biomass TiO_2 nanocomposites," *J. Phys. Conf. Ser.*, vol. 2243, no. 1, October, 2022, doi: 10.1088/1742-6596/2243/1/012077.

[3] M. Diantoro, N. D. Arya, I. Luthfiyah, H. Pujiarti, and S. Maensiri, "Investigating the CoS_2 mass fraction enhancing performance supercapacitor for medium low consumption," *E3S Web Conf.*, vol. 473, pp. 1–11, January, 2024, doi: 10.1051/e3sconf/202447303003.

[4] M. Diantoro, I. Istiqomah, Y. Al Fath, N. Nasikhudin, Y. Alias, and W. Meevasana, "Potential of MnO_2-based composite and numerous morphological for enhancing supercapacitors performance," *Int. J. Appl. Ceram. Technol.*, vol. 20, no. 4, pp. 2077–2098, February, 2023, doi: 10.1111/ijac.14377.

[5] M. Diantoro, N.I.M Aturroifah, I. Luthfiyah, J. Utomo, I. Hamidah, B. Yuliarto *et al*., "3D-porous activated carbon morphological modification of Manihot esculenta tuber and Bambusa blumeana stem for high-power density supercapacitor: Biomass waste to sustainable energy," *Carbon Resour. Convers.*, no.1 , p. 100313, March, 2025, doi: 10.1016/j.crcon.2025.100313.

[6] M. Diantoro, N.I.M Aturroifah, I. Luthfiyah, J. Utomo, I. Hamidah, B. Yuliarto *et al*., "Optimizing sponge-like activated carbon from Manihot esculenta tubers for high-performance supercapacitors," *Arab. J. Chem.*, vol. 18, no. 1, p. 106068, November, 2025, doi: 10.1016/j.arabjc.2024.106068.

[7] J.P. Cao, S. He, Y. Wu, X.Y. Zhao, X.Y. Wei, and T. Takarada, "Synthesis of NiO/activated carbon composites and their application as electrode materials for capacitors," *Int. J. Electrochem. Sci.*, vol. 12, no. 4, pp. 2704–2718, March, 2017, doi: 10.20964/2017.04.39.

[8] F. Mbarki, T. Selmi, A. Kesraoui, and M. Seffen, "Low-cost activated carbon preparation from Corn stigmata fibers chemically activated using H_3PO_4, $ZnCl_2$ and KOH: Study of methylene blue adsorption, stochastic isotherm and fractal kinetic," *Ind. Crops Prod.*, vol. 178, pp. 1–50, April, 2022, doi: 10.1016/j.indcrop.2022.114546.

[9] M. Bora, J. Tamuly, S.M Benoy, S. Hazarika, D. Bhattacharjya, and B.K. Saikia, "Highly scalable and environment-friendly conversion of low-grade coal to activated carbon for use as electrode material in symmetric supercapacitor," *Fuel*, vol. 329, p. 125385, July, 2022, doi: 10.1016/j.fuel.2022.125385.

[10] A. Borenstein, O. Hanna, R. Attias, S. Luski, T. Brousse, and D. Aurbach, "Carbon-based composite materials for supercapacitor electrodes: A review," *J. Mater. Chem. A*, vol. 5, no. 25, pp. 12653–12672, May, 2017, doi: 10.1039/c7ta00863e.

[11] V. Kuzmenko, O. Naboka, M. Haque, H. Staaf, G. Goransson, P. Gatenholm *et al.*, "Sustainable carbon nanofibers/nanotubes composites from cellulose as electrodes for supercapacitors," *Energy*, vol. 90, pp. 1490–1496, June, 2015, doi: 10.1016/j.energy.2015.06.102.

[12] S. Peng, L. Fan, C. Wei, X. Liu, H. Zhang, W. Xu *et al*., "Flexible polypyrrole/copper sulfide/bacterial cellulose nanofibrous composite membranes as supercapacitor electrodes," *Carbohydr. Polym.*, vol. 157, pp. 344–352, February, 2017, doi: 10.1016/j.carbpol.2016.10.004.

[13] P. Kossyrev, "Carbon black supercapacitors employing thin electrodes," *J. Power Sources*, vol. 201, pp. 347–352, November, 2012, doi: 10.1016/j.jpowsour.2011.10.106.

[14] K. Yang, K. Cho, and S. Kim, "Effect of carbon black addition on thermal stability and capacitive performances of supercapacitors," *Sci. Rep.*, vol. 8, no. 1, pp. 1–7, August, 2018, doi: 10.1038/s41598-018-30507-5.

[15] C. Fan, Y. Dong, Y. Liu, L. Zhang, D. Wang, X. Lin *et al.*, "Mesopore-dominated hollow carbon nanoparticles prepared by simple air oxidation of carbon black for high mass loading supercapacitors," *Carbon*, vol. 160, pp. 328–334, January, 2020, doi: 10.1016/j.carbon.2020.01.034.

[16] A. Balducci and C. Schütter, "Carbon blacks as active materials for electrochemical double layer capacitors," *Bol. Grupo Espanol Carbon*, no. 37, pp. 2–5, September, 2015.

[17] C.-M. Wang, C.-Y Wen, Y.-C Chen, J. -Y Chang, C.-W Ho, K.-S Kao *et al.*, "The influence of specific surface area on the capacitance of the carbon electrodes supercapacitor," *Proceedings of the 3rd International Conference on Industrial Application Engineering,* no. 3, pp. 439–442, 2015, doi: 10.12792/iciae2015.077.

[18] M. Ates and O. Kuzgun, "Modified carbon black, CB/MnO_2 and CB/MnO_2/PPy nanocomposites synthesised by microwave-assisted method for energy storage devices with high electrochemical performances," *Plast. Rubber Compos.*, vol. 49, no. 8, pp. 342–356, October, 2020, doi: /10.1080/14658011.2020.1753336.

[19] N. Ahmadi and F. Nugroho, "Influence of biomass based carbon black as filler composite on tensile and impact strength," *Angkasa J. Ilm. Bid. Teknol.*, vol. 12, no. 2, pp. 135–140, November, 2020, doi: 10.28989/angkasa.v12i2.539.

[20] F. Markoulidis, C. Lei, C. Lekakou, D. Duff, S. Khalil, B. Martorana *et al.*, "A method to increase the energy density of supercapacitor cells by the addition of multiwall carbon nanotubes into activated carbon electrodes," *Carbon*, vol. 68, pp. 58–66, August, 2014, doi: 10.1016/j.carbon.2013.08.040.

[21] I. Luthfiyah, A.A Ittikhad, T. Suprayogi, Nasikhudin, M. Diantoro, S. Maensiri *et al.*,

"The effect of concentration PVP on microstructure activated carbon mesoporous and it's potential of activated carbon mesoporous-CB symmetric supercapacitors," in *Proceedings of 2nd International Conference on Renewable Energy (I-CoRE 2021)*, vol. 2687, no. 1, p. 50025, May, 2023, doi: 10.1063/5.0122030.

[22] F. Wang, L. Zhang, Q. Zhang, J. Yang, G. Duan, W. Xu *et al*., "Electrode thickness design toward bulk energy storage devices with high areal/volumetric energy density," *Appl. Energy*, vol. 289, p. 116734, March, 2021, doi: 10.1016/j.apenergy.2021.116734.

[23] C. Young, H.T. Chen, and S.Z. Guo, "Highly porous holey carbon for high areal energy density solid-state supercapacitor application," *Micromachines*, vol. 13, no. 6, June, 2022, doi: 10.3390/mi13060916.

[24] B.J. Choudhury, H.H. Muigai, P. Kalita, and V.S. Moholkar, "Biomass blend derived porous carbon for aqueous supercapacitors with commercial-level mass loadings and enhanced energy density in redox-active electrolyte," *Appl. Surf. Sci.*, vol. 601, p. 154202, March, 2022, doi: 10.1016/j.apsusc.2022.154202.

[25] Z. Chen, X. Wang, W. Li, X. Yang, J. Qiu, and Z. Wang, "A low-temperature dehydration carbon-fixation strategy for lignocellulose-based hierarchical porous carbon for supercapacitors," *ChemSusChem*, vol. 15, no. 1, November, 2022, doi: 10.1002/cssc.202101918.

[26] V. Wardani, L. Rohmawati, W. Setyarsih, D. Alfarisi, and A. Subhan, "Analysis of charging/discharging supercapacitor active carbon/rGO based on natural materials," *J. Phys. Conf. Ser.*, vol. 1491, no. 1, 2020, doi: 10.1088/1742-6596/1491/1/012044.

[27] R. Wang, Y. Qian, W. Li, S. Zhu, F. Liu, Y. Guo *et al.*, "Performance-enhanced activated carbon electrodes for supercapacitors combining both graphene-modified current collectors and graphene conductive additive," *Materials (Basel).*, vol. 11, no. 5, pp. 1–13, May, 2018, doi: 10.3390/ma11050799.

[28] F. Yu, Y. Zhang, Y. Zhang, Y. Gao, and Y. Pan, "Promotion of the degradation perfluorooctanoic acid by electro-Fenton under the bifunctional electrodes: Focusing active reaction region by Fe/N co-doped graphene modified cathode," *Chem. Eng. J.*, vol. 457, p. 141320, December, 2023, doi: 10.1016/j.cej.2023.141320.

[29] F. Wang, G. Li, J. Zheng, J. Ma, C. Yang, and Q. Wang, "Microwave synthesis of three-dimensional nickel cobalt sulfide nanosheets grown on nickel foam for high-performance asymmetric supercapacitors," *J. Colloid Interface Sci.*, vol. 516, pp. 48–56, April, 2018, doi: 10.1016/j.jcis.2018.01.038.

[30] H. Pujiarti, Z.A Pangestu, N. Sholeha, Nasikhudin, M. Diantoro, J. Utomo *et al*., "The effect of acetylene carbon black (ACB) loaded on polyacrylonitrile (PAN) nanofiber membrane electrolyte for DSSC applications," *Micromachines*, vol. 14, no. 2, February, 2023, doi: 10.3390/mi14020394.

[31] R.N.S. Rofika, W. Honggowiranto, H. Jodi, S. Sudaryanto, E. Kartini, and R. Hidayat, "The effect of acetonitrile as an additive on the ionic conductivity of imidazolium-based ionic liquid electrolyte and charge-discharge capacity of its Li-ion battery," *Ionics (Kiel).*, vol. 25, no. 8, pp. 3661–3671, March, 2019, doi: 10.1007/s11581-019-02919-4.

[32] S.S Hegde and B.R Bhat, "Impact of electrolyte concentration on electrochemical performance of cocos nucifera waste-derived high-surface carbon for green energy storage," *Fuel*, vol. 371, no. Part A, p. 131999, September, 2024, doi: 10.1016/j.fuel.2024.131999.

[33] S.J. Rajasekaran, A.N. Grace, G. Jacob, A. Alodhayb, S. Pandiaraj, and V. Raghavan, "Investigation of different aqueous electrolytes for biomass-derived activated carbon-

based supercapacitors," *Catalysts*, vol. 13, no. 2, January, 2023, doi: 10.3390/catal13020286.

[34] Y. Fang, Q. Zhang, and L. Cui, "Recent progress of mesoporous materials for high performance supercapacitors," *Microporous Mesoporous Mater.*, vol. 314, p. 110870, February, 2021, doi: 10.1016/j.micromeso.2020.110870.

[35] N. Mohammadi, K. Pourreza, N.B Adeh, and M. Omidvar, "Defective mesoporous carbon/MnO2 nanocomposite as an advanced electrode material for supercapacitor application," *J. Alloys Compd.*, vol. 883, p. 160874, November, 2021, doi: 10.1016/j.jallcom.2021.160874.

[36] M. Usman, M.T Ahsan, S. Javed, Z. Ali, Y. Zhan, I. Ahmed *et al*., "Facile synthesis of iron–nickel–cobalt ternary oxide (FNCO) mesoporous nanowires as electrode material for supercapacitor application," *J. Mater.*, vol. 8, no. 1, pp. 221–228, January, 2022, doi: 10.1016/j.jmat.2021.03.012.

[37] D. Wang, Z. Pan, and Z. Lu, "From starch to porous carbon nanosheets: Promising cathodes for high-performance aqueous Zn-ion hybrid supercapacitors," *Microporous Mesoporous Mater.*, vol. 306, p. 110445, June, 2020, doi: 10.1016/j.micromeso.2020.110445.

[38] R. Ali, Z. Aslam, R.A. Shawabkeh, A. Asghar, and I. A. Hussein, "BET, FTIR, and RAMAN characterizations of activated carbon from waste oil fly ash," *Turkish J. Chem.*, vol. 44, no. 2, pp. 279–295, April, 2020, doi: 10.3906/KIM-1909-20.

[39] A.I. Bakti and P.L. Gareso, "Characterization of active carbon prepared from coconuts shells using FTIR, XRD and SEM techniques," *J. Ilm. Pendidik. Fis. Al-Biruni*, vol. 7, no. 1, p. 33, April, 2018, doi: 10.24042/jipfalbiruni.v7i1.2459.

[40] J. Zhang, J. Sun, T.A. Shifa, D. Wang, X. Wu, and Y. Cui, "Hierarchical MnO_2/activated carbon cloth electrode prepared by synchronized electrochemical activation and oxidation for flexible asymmetric supercapacitors," *Chem. Eng. J.*, vol. 372 , pp. 1047–1055, January, 2019, doi: 10.1016/j.cej.2019.04.202.

[41] D.V. Chernysheva, N.V. Smirnova, and V.P. Ananikov, "Recent trends in supercapacitor research: Sustainability in energy and materials," *ChemSusChem*, vol. 17, no. 5, November, 2024, doi: 10.1002/cssc.202301367.

[42] Y. Liu, H. Chen, and L. Li, "Applications and challenges of porous carbon with different dimensions in supercapacitors—a mini review," *Front. Energy Res.*, vol. 10, August, pp. 1–19, August, 2022, doi: 10.3389/fenrg.2022.951701.

[43] E.S. Appiah, K.M-Darkwa, A. Andrews, F.O Agyemang, M.A Nartey, K. Makgopa *et al.*, "Tailoring a hierarchical porous carbon electrode from carbon black via 3D diatomite morphology control for enhanced electrochemical performance," *Nanoscale Adv.*, vol. 6, no. 24, pp. 6265–6277, September, 2024, doi: 10.1039/d4na00680a.